THE JOURNAL OF PHYSICAL CHEMISTRY C

Article

pubs.acs.org/JPCC

The Effect of Metal−Cation Vacancies on Vanadium Antimonate Surface Properties. A Theoretical Study

Hernán Seitz,[†] Alfredo Juan,[†,*] Graciela Brizuela,[†] and Beatriz Irigoyen[‡]

[†]Departamento de Física and IFISUR (UNS-CONICET), Avda Alem 1253, B8000CPB Bahía Blanca, Argentina

[‡]Departamento de Ingeniería Química, Universidad de Buenos Aires, Pabellón de Industrias, Ciudad Universitaria, C1428EGA Ciudad Autónoma de Buenos Aires, Argentina

ABSTRACT: In this work, we studied the distribution of V and Sb vacancies in the rutile-type vanadium antimonate phase and the influence of these cationic defects on the $VSbO_4(110)$ surface properties. We performed density functional theory (DFT) calculations to compute the energy stability of bulk supercells with different geometrical arrangements of the metal-cation-deficient sites. Then, we built a model of the nonstoichiometric $VSbO_4(110)$ surface, which exhibited an extra O layer and isolated V cations—V atoms surrounded by Sb ions—that could act as Lewis acid sites. The density of states (DOS) plot of this surface showed contributions of O(2p) states, coming from surface O atoms nearest-neighbor of a V vacancy, and V(3d) states near the Fermi level. We also studied the influence of cation-vacancies in the formation of Brønsted acid sites.

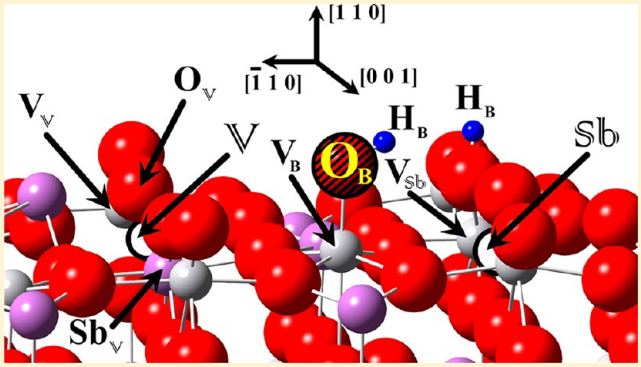

1. INTRODUCTION

V−Sb mixed oxides are recognized as active and selective catalysts for several oxidation processes. These catalysts are used for the selective destruction of nitrogen organic volatile compounds,[1] and the oxidation of hydrogen sulfide to sulfur,[2,3] methane to formaldehyde,[4] and isobutene to methacrolein.[5] V−Sb mixed oxides are also the preferred catalysts for the oxidation of propylene or propane in order to obtain acrylonitrile.[6−11] Acrylonitrile is an important component used in the manufacture of thermoplastic resins and acrylic fibers, and is mostly obtained by ammoxidation of propylene. In the past few years, the production of acrylonitrile by ammoxidation of propane has also attracted great attention due to the low price of this hydrocarbon compared to that of propylene.

The $VSbO_4$ oxide was initially synthesized by Birchall and Sleight, who observed a rutile-type tetragonal structure.[12] From a formal point of view, V and Sb cations would be present in the $VSbO_4$ phase as V^{3+} and Sb^{5+}, respectively. However, it has been reported that the $VSbO_4$ structure presents 16% of cationic defects, leading to the presence of vanadium cations in V^{4+} the oxidation state.[13] The formation of a cation-deficient rutile-type $VSbO_4$ phase, with the $V_{0.64}{}^{4+}V_{0.28}{}^{3+}Sb_{0.92}{}^{5+}\square_{0.16}O_4{}^{2-}$ formula (the square □ represents the cation vacancies), has been connected with the activity of the V−Sb catalysts.[13] In this sense, the presence of metal−cation defects promotes the formation of redox couples V^{4+}/V^{3+} thus enhancing the catalytic activity of the vanadium antimonate in valuable hydrocarbon selective oxidation reactions.[14,15] The isolation of vanadium sites at the surface of this catalyst has also been related to the high activity and selectivity of the $VSbO_4$ phase in propane ammoxidation reactions to acrylonitrile.[14,16−18]

The catalytic behavior of V−Sb mixed oxides has also been evaluated from a theoretical point of view, by performing quantum chemical calculations.[19−22] Toluene adsorption reactions on the stoichiometric $VSbO_4(110)$ surface were studied with a tight-binding approach.[19,20] This methodology was also used to evaluate the $VSbO_4(110)$ surface reduction−oxidation process.[22] More recently, ammonia adsorption reactions on a similar perfect (110)-surface model have been evaluated using the density functional theory (DFT).[21] The interactions of light hydrocarbons have also been studied on the stoichiometric $VSbO_4(110)$ surface as well as the same slab with a surface Sb vacancy.[14]

On the other hand, it is worth noticing that ammoxidation of hydrocarbons on V−Sb mixed oxides requires the adsorption of NH_3-derived species and thus involves the participation of Brønsted and Lewis acid sites.[21] These sites have active roles not only in vanadium antimonate oxides, but also in other compounds such as zeolites,[23] mordenites,[24] or V_2O_5/TiO_2 catalysts.[25] With regard to the $VSbO_4(110)$ surface, it has been reported that isolated V sites—V atoms surrounded by Sb ions—are the Lewis acid sites involved in the preferential adsorption of NH_3, thus providing a unique local environment for ammoxidation reactions.[21] Meanwhile, the model for

Received: April 2, 2013
Revised: September 11, 2013
Published: September 13, 2013

   dx.doi.org/10.1021/jp4032805 | J. Phys. Chem. C 2013, 117, 20548−20556

Brønsted acid sites was built by formal adsorption of water as OH^-, put on top of the Lewis site, and H^+, put on top of the bridging oxygen row.[21]

Despite the important influence of metal−cation vacancies in the catalytic behavior of V−Sb mixed oxides, as far as we know only stoichiometric $VSbO_4$(110) surface model slabs have been used for studying their performance from a fundamental point of view. In this way, it would be interesting to model the crystalline structure of the nonstoichiometric $VSbO_4$ phase and the catalytic surface active sites. This model will be useful for studying the interactions of different hydrocarbons and intermediate species on the V−Sb mixed oxide surface. In addition, a quantum-chemical study of the formation of cation vacancy sites, Sb and V defects, in the rutile-type structure and that of surface isolated V cations could provide clues at the atomic level, that would help to better understand the catalytic behavior of the $VSbO_4$ active phase. Thus, in this work we carried out periodic density functional theory (DFT) calculations in order to study the distribution of V and Sb vacancies in the $VSbO_4$ rutile-type structure and their effect on the formation of Lewis acid sites—surface isolated V sites—and Brønsted acid sites.

2. THEORETICAL METHODS AND MODELS

2.1. Calculation Details. In this paper, we reported quantum chemical calculations carried out with self-consistent DFT theory as implemented in the Vienna Ab-Initio Simulation Package (VASP).[26−28] Kohn−Sham equations were solved with the generalized gradient approximation (GGA) using the exchange-correlation functional PW91.[29] Core electrons were represented with the projector augmented wave (PAW) method.[30] Valence electrons V($4s^2$, $3d^3$), Sb($5s^2$, $5p^3$), and O($2s^2$, $2p^4$) were described by plane waves, and we used a truncation energy value of 408 eV. Tolerance for the total free energy change was set in 10^{-3} eV. For geometry optimizations and total energy calculations, we applied the Gaussian smearing scheme with a smearing width of 0.2 eV and used spin polarization in all cores. The calculations were performed with a large 2 × 2 × 1 supercell, derived from the trirutile-type conventional cell.

The 16% cation-defective $VSbO_4$ bulk was simulated by introducing two metal-cation (Sb and V) vacancies in the 2 × 2 × 1 supercell. In this way, the integrals over the Brillouin zone were sampled using a 3 × 3 × 2 k-points grid according to the Monkhorst−Pack scheme.[31]

The nonstoichiometric $VSbO_4$(110) surface was modeled with a slab of 13.316 × 9.286 × 28 $Å^3$; which consisted in 12 atomic layers and a vacuum space of about 15 Å, to avoid interactions between successive images. The surface supercell was formed by 22 V cations, 22 Sb cations, and 96 oxygen atoms. The Brillouin zone was sampled using a Monkhorst-Pack grid of 2 × 3 × 1 k-points. For all energy calculations, the atomic positions of adsorbates and V, Sb, and O ions located in the six uppermost layers of the slab were relaxed; while those of the six lowermost layers ions were kept fixed to their bulk positions.

The atom projected density of states (PDOS) was calculated by projecting one-electron states onto spherical harmonic atomic orbitals centered on atomic sites. A qualitative study of the bonding between different atoms was also performed using the Overlap Population (OP) concept,[32] as implemented in the SIESTA code.[33] We calculated the OP of V−O and Sb−O bonds in the cation-deficient $VSbO_4$ bulk and (110) surface models. To present complete information, we also reported those OPs for stoichiometric structures.

2.2. The $VSbO_4$: Bulk, Surface, and Acid Sites Models. $VSbO_4$ has a rutile-type tetragonal structure.[12] The rutile structure is formed by infinite chains of metal−oxygen octahedrons with shared edges and corners. In this structure, each metal center binds to six oxygen atoms (O) while each oxygen atom binds to three metal atoms (M). Metal−metal distances in the resulting structure of coordination 6:3 are always relatively long and there is no effective O···O or M···M interactions. Additionally, open channels parallel to *c*-axis are formed in the crystal.

In our theoretical approach, we first studied the $VSbO_4$ rutile structure with a stoichiometric composition. The bulk was modeled with a trirutile supercell (see Figure 1) containing the most probable metal−oxygen combinations as reported from powder diffraction studies.[13] The calculated lattice parameters for this $VSbO_4$ trirutile-type structure: $a = b = 4.708$ Å and $c' = 9.286$ Å (where $c' = 3c$, $c = 3.095$ Å), are in good agreement with the corresponding experimental XRD data.[34]

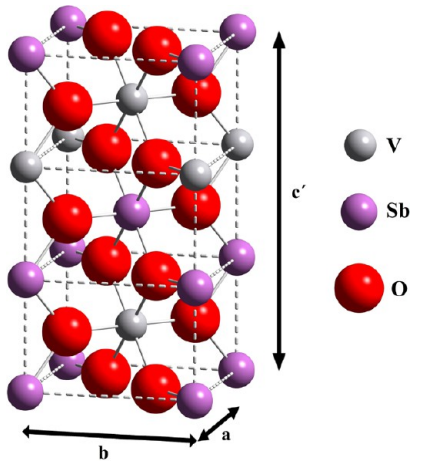

Figure 1. (a) Trirutile-type tetragonal $VSbO_4$ structure.

The stoichiometric $VSbO_4$(110) surface was generated by cutting the bulk solid with the ideal (110) plane and retaining an extra O-layer.

Then, we studied the $VSbO_4$ cation-deficient phase by modeling bulk superstructures that are representative of the reported formula $V_{0.92}Sb_{0.92}\square_{0.16}O_4$.[13] These supercells (see Figure 2a−e) were formed by 12 rutile-type unit cells, which include 16.67% of Sb and V cation vacancies, and represent five different combinations of V and Sb vacancies. From these supercells, we built the nonstoichiometric (110) surface, as it appears to be the most stable rutile face and it results from breaking the smallest number of M−O bonds.

Finally, we explored the formation of Lewis and Brønsted acid sites. In the case of a Lewis site, we considered a surface isolated V cation in the higher oxidation state, which provides a unique local environment for the ammoxidation reactions as reported from experimental and theoretical results.[21] The most stable Brønsted site configuration was found by computing the adsorption energy of H and OH species in two sequences. On the one hand, we calculated the adsorption energy of H species on different O-metal sites, and then, that of OH species on the most stable protonated surface. On the other hand, we first

dx.doi.org/10.1021/jp4032805 | J. Phys. Chem. C 2013, 117, 20548−20556

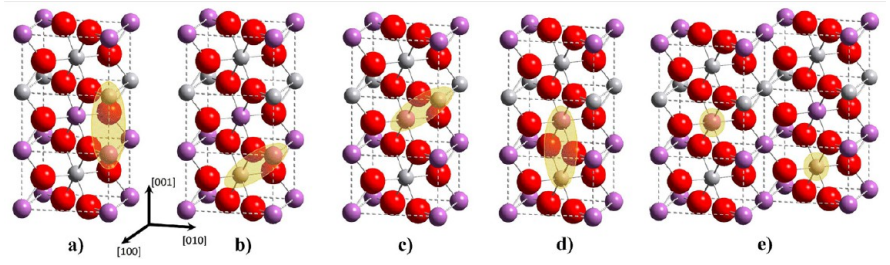

Figure 2. Supercells showing the five different combinations of V and Sb vacancies in the bulk.

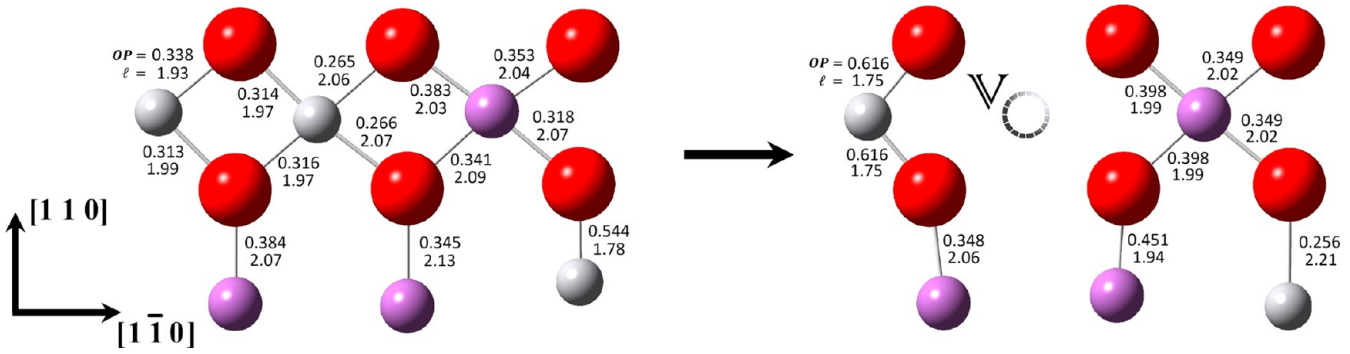

Figure 3. Bond distances (l) and overlap population (OP) values for selected V−O and Sb−O bonds close to a V-vacancy in the $VSbO_4$ bulk structure (stoichiometric solid, left; nonstoichiometric solid, right).

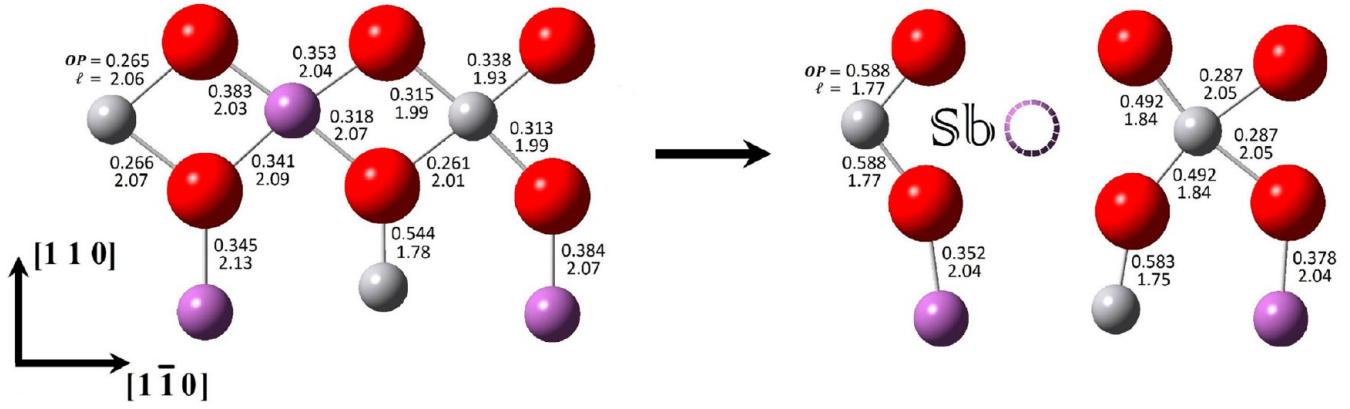

Figure 4. Bond distances (l) and overlap population (OP) values for selected V−O and Sb−O bonds close to a Sb-vacancy in the $VSbO_4$ bulk structure (stoichiometric solid, left; nonstoichiometric solid, right).

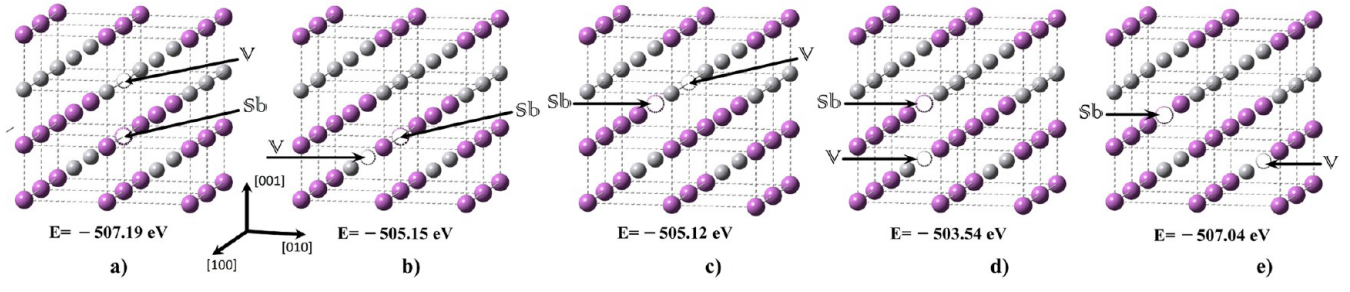

Figure 5. Schematic representation of the five optimized nonstoichiometric $VSbO_4$ bulk structures with the corresponding energy values. The oxygen atoms were omitted for the sake of clarity.

evaluated the interactions of the OH group, and then, those of the H atom on the most stable hydroxilated surface.

To identify the V and Sb vacancies and the atoms located near a V or Sb vacancy or next to a Brønsted site we use different labels. The Sb and V vacancies were indicated with white circles and labeled as $\mathbb{S}\mathrm{b}$ and $\mathbb{V}$, respectively. The atoms located near a V vacancy ($\mathbb{V}$) were labeled as $V_{\mathbb{V}}$, $Sb_{\mathbb{V}}$ and $O_{\mathbb{V}}$, and those near a Sb vacancy ($\mathbb{S}\mathrm{b}$) as $Sb_{\mathbb{S}\mathrm{b}}$, $V_{\mathbb{S}\mathrm{b}}$ and $O_{\mathbb{S}\mathrm{b}}$. The atoms located near the Brønsted site were labeled as Sb_B, V_B and O_B.

dx.doi.org/10.1021/jp4032805 | J. Phys. Chem. C 2013, 117, 20548−20556

3. RESULTS AND DISCUSSION

3.1. The Bulk Structures. The stoichiometric $VSbO_4$ bulk structure was modeled with the supercell shown in Figure 1. After relaxing the Sb, V, and O atomic positions in this supercell, the length of V−O bonds ranged from 1.78 to 2.07 Å, while those of Sb−O bonds from 2.03 to 2.13 Å. Meanwhile, the overlap population (OP) values of those V−O and Sb−O bonds were in the range of 0.54 to 0.27 and 0.34 to 0.38, respectively. The bond lengths and overlap population values of selected V−O and Sb−O bonds were indicated in Figures 3 and 4, left sides (see the stoichiometric $VSbO_4$ bulk structure).

The cation-deficient bulk structure, of which the reported formula is $V_{0.92}Sb_{0.92}\square_{0.16}O_4$,[13] was modeled with supercells formed by 12 rutile-type unit cells. These supercells include 16.67% of metal−cation (V and Sb) vacancies distributed in five different combinations (see Figures 2a−e), and were optimized by relaxing all the Sb, V, and O atomic positions. The schematic representation of the five optimized non-stoichiometric $VSbO_4$ bulk structures and the corresponding calculated total energy values were shown in Figure 5a−e. Comparison of these energy values indicated that configurations 5a and 5e are the most stable.

We then studied the effect of the cation-vacancies (V and Sb) in the V−O and Sb−O bond lengths and overlap population (OP) values of their nearest-neighbor V and Sb atoms. The V cation located near a V vacancy shortened its V−O bond lengths up to 12%, compared with those in the stoichiometric bulk structure (see Figure 3: 1.75 Å and 1.99 Å, respectively). Consequently, these V−O bonds almost duplicated their OP values. On the other hand, the Sb cation nearest-neighbor to a V vacancy was less affected, and the calculations showed that its Sb−O bond lengths diminished 1% compared to those for the stoichiometric bulk. Meanwhile, the corresponding OP values increased about 6%.

When considering the effect of the Sb vacancies on their nearest-neighbor atoms, our analysis showed that the closer V cation diminished its V−O bond lengths up to 14% compared to those for the stoichiometric bulk (see Figure 4: 2.07 Å and 1.77 Å, respectively). Accordingly, the corresponding OP(V−O) values were almost duplicated. The changes in Sb−O bond lengths and OP values of Sb cations located near to a Sb defect were subtle. They showed a stretching of 1% while the OP values changed about 9%.

3.2. The Nonstoichiometric Surface Structure. Considering the preferred cation deficient $VSbO_4$ bulk supercells of Figure 5 panels a and e, we found that the most stable nonstoichiometric (110) surface was the one resulting from configuration 5e. The optimized $VSbO_4$(110) surface is shown in Figure 6. The nonstoichiometric $VSbO_4$(110) surface model shows an extra oxygen plane and presents different O-metal local arrangements -$OSb_2\square$, $OSbV\square$, and $OV_2\square$ (notice that the square $\square$ denotes cation vacancies), in agreement with those reported in ref 13. The catalytic performance of the $VSbO_4$ rutile-type phase in hydrocarbon (amm)oxidation reactions has been related to the presence of surface isolated V sites (V cations surrounded by Sb ions),[6,16,17,21] and also to that of cationic vacancies.[14,18,35] Therefore, we underline that our nonstoichiometric $VSbO_4$(110) surface model shows some V and Sb vacancies located close to the surface, covered by the extra oxygen plane, while others are in the inner layers (see Figure 6, Sb and V vacancies are indicated with white circles). In addition, this surface shows a V cations configuration

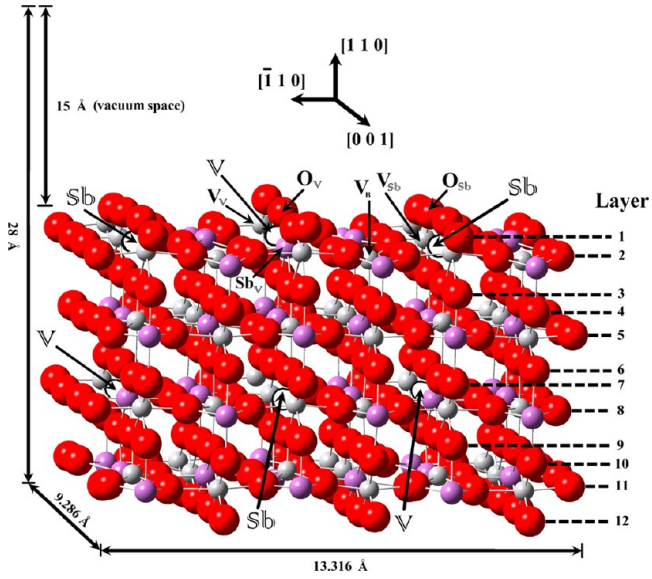

Figure 6. The nonstoichiometric $VSbO_4$(110) surface.

separated by Sb ions representing the "site isolation" concept.[36,37]

The introduction of V and Sb vacancies resulted in stretching of the nearest-neighbor cation metal-O bonds. The details of the V−O and Sb−O bond lengths and their corresponding OP values in the proximity of a V vacancy are shown in Figure 7, while those in the proximity of Sb defects are shown in Figure 8. In order to present complete information, we also included those values for the stoichiometric $VSbO_4$(110) surface (see Figures 7 and 8, left side).

The V cations located near a V-vacancy (see Figure 7: VV), shortened their V−O bonds up to 12% and subsequently reinforced their OP up to 81%. The Sb cations close to a V defect (see Figure 7, Sb_V), diminished the Sb−O distances about 22% and increased their OP values. Note that more distant Sb−O bonds were also shortened (3%).

In addition, geometric distortion in the vicinity of the Sb defects was very important. Neighboring V cations (see Figure 8, V_{Sb}), shortened their V−O bonds about 12% with an increase of the OP values of about 90%. The changes in the Sb−O bond lengths and OP values of the surrounding Sb cations were subtle.

3.3. Electronic Structure of Surface Containing Vacancies. The total DOS of the bare $V_{0.92}Sb_{0.92}\square_{0.16}O_4$(110) surface is shown in Figure 9. This plot presents O, V, and Sb bands located at different energy values. Between −21 and −17 eV the DOS curve was mainly formed by Sb(5s), Sb(5p), and V(3d) orbitals. In this energy region, the mentioned orbitals contributed in similar proportions. The small band between −12 and −8 eV was originated from Sb(5s) orbitals. The top of the band, between −8 eV and the Fermi level, was mainly composed of O(2p) orbitals (O−metal bonds) and V(3d) states, while the contribution of Sb(5p) orbitals was quite small. The peak at −1 eV corresponded to V(3d) orbitals. The contributions from Sb(5s), Sb(5p), and O(2p) orbitals can be seen above the Fermi level.

Although the $VSbO_4$ phase is rutile-type, our DOS calculations did not reflect the characteristic band gap of TiO_2 (rutile) but the picture of vanadium dioxide (VO_2) with rutile-like structure.[38,39]

dx.doi.org/10.1021/jp4032805 | J. Phys. Chem. C 2013, 117, 20548−20556

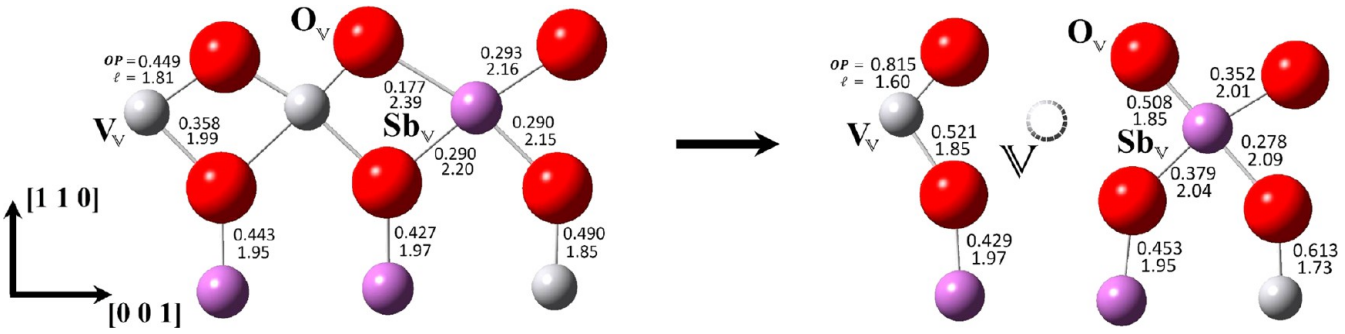

Figure 7. Bond distances (l) and overlap population (OP) values for selected V−O and Sb−O bonds close to a V-vacancy in the $VSbO_4(110)$ surface (stoichiometric solid, left; nonstoichiometric solid, right).

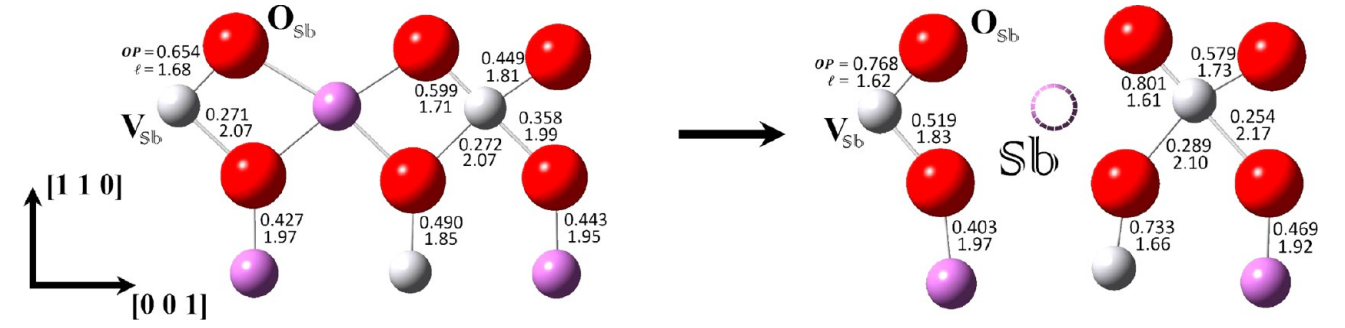

Figure 8. Bond distances (l) and overlap population (OP) values for selected V−O and Sb−O bonds close to a Sb-vacancy in the $VSbO_4(110)$ surface (stoichiometric solid, left; nonstoichiometric solid, right).

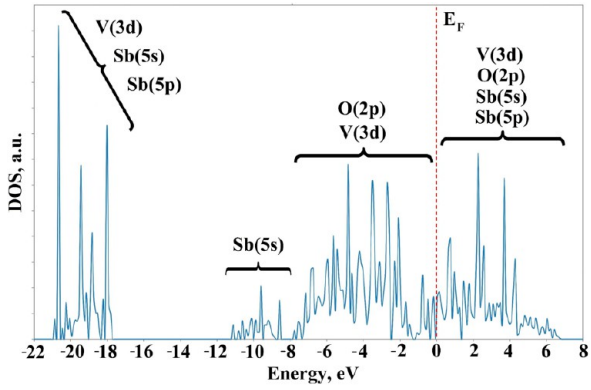

Figure 9. Total DOS of the $V_{0.92}Sb_{0.92}\square_{0.16}O_4(110)$ surface.

Haras et al.,[38] computed electronic properties of the rutile-$VO_2(110)$ surface by using DFT calculations. They showed that the V(3d) band is located in the region from −2 to 0 eV. At about 2 eV below the highest occupied molecular orbital (HOMO), the DOS curve presents a decrease and then it starts to increase again at 1 eV below the HOMO. This density is attributed to 5- and 6-fold coordinated V cations. The DOS of the unoccupied levels remains finite above the HOMO reflecting the metallic character of the surface.[38] The electronic calculation for bulk VO_2 performed by Guelfucci et al.,[39] is in good agreement with the XPS spectra reported by Werthein.[40] This measured O(2p) band consists of two main structures, which are in the same energy region reported by Haras et al.[38] The XPS spectra also presents an intense peak below −20 eV, which corresponds to O(2s) weakly mixed with O(2p) and V(3d) states.[40] Note that in our model of the non-stoichiometric $VSbO_4(110)$ surface, the DOS plot is dominated by O(2p) contributions in the valence band region between −2 and −8 eV. Recently, Mellan and Grau-Crespo[41] reported VASP-DFT calculations of rutile VO_2 surfaces. The plot of their DOS in the region from −8 to 0 eV is in agreement with our results thus providing additional support for the electronic similarities between the $VSbO_4(110)$ and the VO_2 (rutile) surfaces.

Figure 10 shows the DOS curves of selected surface O atoms, which are located near a V vacancy ($O_{\mathbb{V}}$, see insert) or a Sb vacancy ($O_{\mathbb{Sb}}$, see the insert). In this plot, it can be seen that the $O_{\mathbb{V}}$ atom presents a band of O(2p) states near the Fermi level with a sharp peak at −1 eV. Note that at this energy value there are also V(3d) contributions. For the $VSbO_4$ phase, it has been shown that the presence of isolated surface vanadium site is the key factor required for achieving high activity and selectivity in propane ammoxidation reactions.[16−18] In particular, the activity appears to be related to the creation of highly active oxygen sites for the activation of propane.

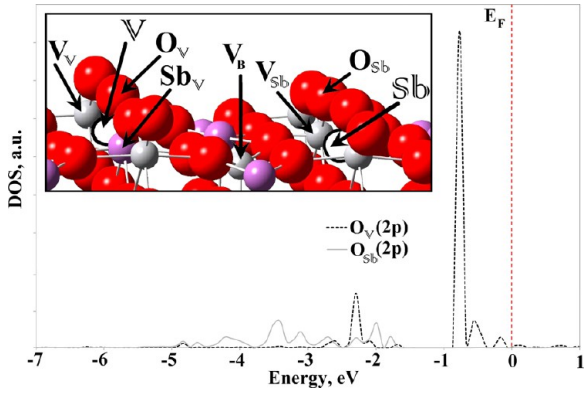

Figure 10. Projected DOS of selected surface O anions ($O_{\mathbb{V}}$ and $O_{\mathbb{Sb}}$).

dx.doi.org/10.1021/jp4032805 | J. Phys. Chem. C 2013, 117, 20548−20556

Moreover, the presence of cationic vacancies is related to that of V^{4+}, which may also be involved through charge transfer in the formation of active oxygen species for the first step of propane activation.[18] Therefore, these $O_{\square}(2p)$ states located near the Fermi level in the DOS plot of our nonstoichiometric $VSbO_4(110)$ surface suggested that surface oxygen like the $O_{\square}$ atom could be involved in the activation of hydrocarbons.

We also analyzed the electronic characteristics of the more distorted surface Sb−O and V−O bonds, due to the formation of cation vacancies. The $Sb_{\square}$—$O_{\square}$ bond (see the local geometry in Figure 7) was distorted due to the presence of the V vacancy. Figure 11 shows the projected DOS curves of

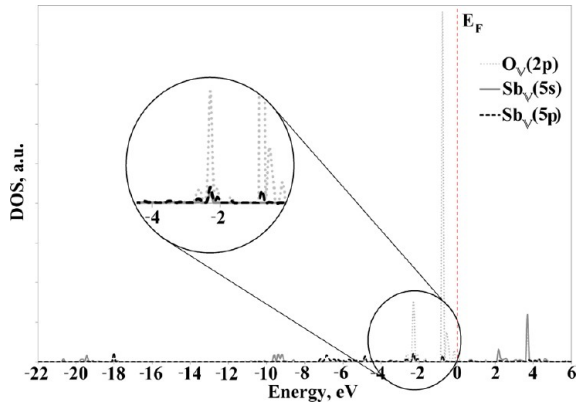

Figure 11. Projected DOS of $Sb_{\square}$ and $O_{\square}$ surface species (as indicated in the insert in Figure 10).

$Sb_{\square}$ and $O_{\square}$ atoms. The projected DOS plot shows a small band around −2 eV, formed mainly by $Sb_{\square}(5p)$ and $O_{\square}(2p)$ orbitals. The $O_{\square}$ atom shows O(2p) states available that are close to the Fermi level, which do not contribute to the $Sb_{\square}$—$O_{\square}$ bond. Figure 12, presents an analogous picture for

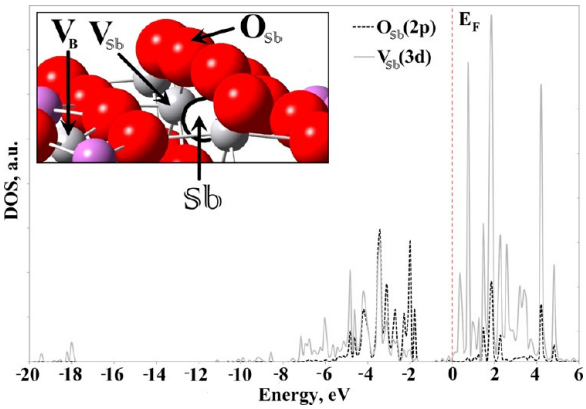

Figure 12. Projected DOS of O_{Sb} and V_{Sb} surface species.

the V_{Sb}—O_{Sb} bond (see the local geometry in Figure 8). We observed $V_{Sb}(3d)$ and $O_{Sb}(2p)$ contributions between −6 and −2 eV, that originate the V_{Sb}—O_{Sb} bond. Note the absence of $O_{Sb}(2p)$ contributions close to the Fermi level.

3.4. Acid Sites on Surface Containing Cation-Vacancies. V−Sb oxide based materials are recognized for their high catalytic performance in C3 hydrocarbons ammoxidation reactions to acrylonitrile. The incorporation of NH_3-derived adsorbed species could involve the participation of surface Lewis or Brønsted acid sites. Rojas et al.,[21] performed a DFT study of ammonia interactions on the $VSbO_4(110)$ surface and showed that NH_3 and NH_2 adsorbed on isolated surface V cations, which act as Lewis sites and provide a unique local environment for the ammoxidation reactions. An experimental spectroscopy study has indicated that NH_3 chemisorbed on Lewis and Brønsted sites, influencing the reactivity of the catalyst surface toward selective hydrocarbon ammoxidation reactions.[42] Therefore, taking into account these indications, we studied the formation of Lewis and Brønsted acid sites on the nonstoichiometric $VSbO_4(110)$ surface.

Figure 6 shows that the nonstoichiometric $VSbO_4(110)$ surface presents isolated V cations surrounded by Sb ions. These V cations are low-coordinated, and thus, can act as Lewis acid sites. In a previous semiempirical study, we evaluated the influence of cationic vacancies in the oxidation state of neighboring isolated V cations[22] and found indications that the formation of cationic defects could stabilize these cations in a higher oxidation state. Experimental reports also indicated that the formation of cationic vacancies in vanadium antimonate reflects in the presence of V^{4+} cations, leading to the following composition: $V_{0.28}{}^{3+}V_{0.64}{}^{4+}Sb_{0.92}{}^{5+}\square_{0.16}O_4$.[13,15] Therefore, we calculated the electronic charge on V atoms by using the Bader Charge analysis.[43] The contribution of O(2p) states, which usually have very little net electron spin, was filtered by integrating the spin charge density. The calculations showed a charge of 2.54e and a spin magnetization of 0.03 μ_B for the V_B cation (see V_B in Figure 6). There are 14 additional V cations with charges ranging between 2.42 and 2.55e and spin magnetization values between 0.01 and 0.37 μ_B. Thus, based in the experimentally reported formula $V_{0.64}{}^{4+}V_{0.28}{}^{3+}Sb_{0.92}{}^{5+}\square_{0.16}O_4{}^{2-}$, we assigned a (4+) oxidation state to those oxidized V cations. The surface isolated V_B cation is surrounded by Sb ions (see Figure 6: Sb−Sb−V−Sb surface cationic chains), and shows a diminished O-coordination. This V cation formed V−O bonds of different lengths: 1.66 Å (1), 1.8 Å (2), and 2.02 Å (2). Notice that V cations showed regular octahedral coordination in the stoichiometric surface (distance (V−O) = 2.02 Å). On the other hand, there are seven V cations with charges ranging between 2.65 and 2.80e and spin magnetization values between 0.92 and 1.5 μ_B. Then, considering Sb cations as Sb^{5+}, we assigned a (3+) oxidation state to those reduced V cations in order to maintain the electroneutrality of the solid.

Starting from the stoichiometric solid, the formally assigned charges were $V^{3+}Sb^{5+}O_4{}^{2-}$.[12] After introducing cation vacancies, the Bader charge analysis shows that, 15 V ions (of a total of 24 vanadium atoms originally presented in the stoichiometric surface slab) are in a higher oxidation state (V^{4+}) allowing us to calculate an approximated $V_{0.625}{}^{4+}V_{0.292}{}^{3+}Sb_{0.916}{}^{5+}\square_{0.167}O_4{}^{2-}$ composition for the nonstoichiometric slab. This composition is in good agreement with that corresponding to the experimental $V_{0.64}{}^{4+}V_{0.28}{}^{3+}Sb_{0.92}{}^{5+}\square_{0.16}O_4{}^{2-}$ formula.[13] Thus, our findings indicated that the introduction of cation-defects in the rutile-type $VSbO_4(110)$ structure facilitated the formation of surface isolated V^{4+} cations (V cations surrounded by Sb ions), considered as Lewis acid sites, forming the V^{4+}/V^{3+} redox couples. Experimentally, these characteristics are recognized as essential for promoting hydrocarbon ammoxidation reactions on a $VSbO_4$ catalyst. Vanadium antimonate catalysts are multifunctional in nature and present several key properties, including different active sites. To achieve the desired product selectivity, the individual active sites must be spatially isolated

dx.doi.org/10.1021/jp4032805 | J. Phys. Chem. C 2013, 117, 20548−20556

from each other and able to dissociate dioxygen and incorporate it into the solid catalyst lattice.[37] The active sites of antimony-based selective alkenes oxidation catalysts are composed of bridging oxygen atoms associated with Sb^{3+}, related to α-H abstraction, and Sb^{5+}, related to oxygen insertion into the hydrocarbon fragment, cations.[1] As a consequence, a reduced surface site is formed, which is subsequently reoxidized via lattice oxygen coming from an adjacent reoxidation site. Grasselli,[44] ascribed that function to V^{4+} cations in antimonate-based catalysts. Centi et al.,[35] compared the structure, surface, and reactivity characteristics for different samples of rutile Sb–V oxides in propane to acrylonitrile ammoxidation reaction and established a correlation between nonstoichiometry of the catalyst and its reactivity. Larrondo et al.,[15] studied the catalytic oxidation of toluene on vanadium antimonate oxides and showed that the selectivity to benzaldehyde could be correlated with the redox properties of the solids. Vanadium sites (V^{4+}) were involved in the incorporation of gaseous oxygen as lattice oxygen and hold the Sb sites in an oxidation state (Sb^{5+}) high enough to insert the lattice oxygen into the hydrocarbon molecule.

On the other hand, Brønsted acid sites in vanadium antimonate catalysts are typically considered as vanadium-based V–OH groups formed via a dissociative water adsorption reaction. Thus, we found the optimum locations of the H and OH groups by performing two-step energy structure relaxations on our surface model. It is reasonable to speculate that the origin of this H and OH species is water that dissociates on the surface. The role of water dissociation on rutile $TiO_2(110)$ surface was described in detail by Hammer et al.[45] STM images of water molecules adsorbed on Ti sites on this surface show a capping hydrogen bridging oxygen and then forming two OH groups. If the surface presents some oxygen vacancies, STM indicates that water dissociates on these sites leaving an OH group on the vacancy and the H locates again in the neighboring bridging oxygen. This mechanism was also reported on the rutile $TiO_2(001)$ surface.[46] Miao et al.[47] studied water activation on a stoichiometric rutile $TiO_2(110)$ surface. They also found that the most stable configuration is the one in which one OH binds to a surface Ti cation while the H binds to a bridging O and this is in agreement with previous calculations.[48,49] It must be pointed out that our study does not include a water dissociation reaction because we are interested in the final OH and H adsorbed species that form the Brønsted site. According to the previous mentioned results, we have two possibilities for H and OH coadsorption, depending on which species is adsorbed first. We found that the sequence of coadsorption influences the stability of the final configuration.

First, we studied the adsorption of an H atom on different surface sites: O, Sb, and V atoms. The adsorption energy ($\Delta E_{ads,H}$) was calculated as the difference between the energy of the $V_{0.92}Sb_{0.92}\square_{0.16}O_4(110)$ surface with an adsorbed H atom ($E_{H/Surf}$) and the energies of the clean surface (E_{Surf}) and the hydrogen molecule in the vacuum (E_{H2}):

$$\Delta E_{ads,H} = E_{H/Surf} - E_{surf} - \frac{1}{2}E_{H2}$$

After relaxation of the structures corresponding to an H atom located on the different surface sites, we found that the H interaction on the V cation was repulsive and that on the Sb cation was of nonbonding character. On the other hand, H adsorption on O_V—Sb_V site (close to a V vacancy) was exothermic ($\Delta E_{ads,H}$ = −2.32 eV), forming a H-(O_V—Sb_V) bond of 0.98 Å length. This H interaction was 1.62 eV more favorable than that on the O–V moiety. Then, we evaluated the adsorption of the OH group on the protonated surface by testing its interactions on different Sb and V cation surface sites. Our calculations indicated favorable OH interactions on Sb and V cations, the adsorption on a V cation being slightly more exothermic than on a Sb cation (~0.20 eV). The OH group bound to this oxidized surface V cation through its oxygen (d(O–V) = 1.79 Å), while the V atom was moved 0.55 Å out of the subsurface (see Figure 13).

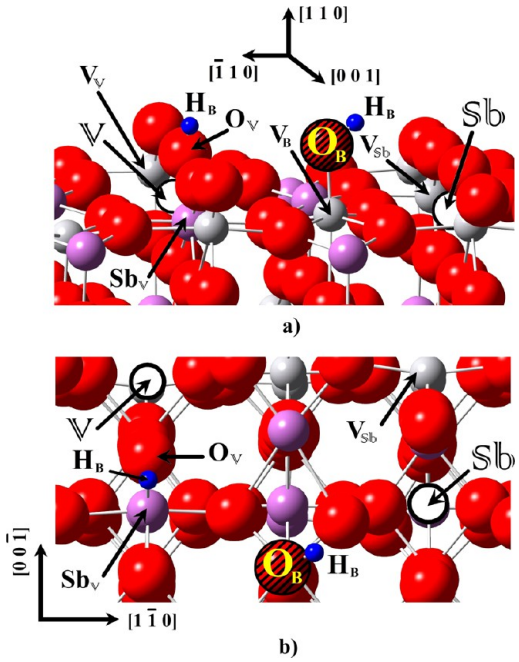

Figure 13. Brønsted acid site formation: (a) side view, (b) top view. Sequence H (1st) then OH.

Considering the second sequence, we started with the adsorption of an OH species. The interaction of the OH group on a V cation was 0.53 eV more stable than that on a Sb cation. After that, we adsorbed the H on this hydroxilated surface. Our calculations indicated that H is preferentially adsorbed on a O_{Sb}—Sb_{Sb} site (see Figure 14). This second possibility was 0.20 eV more stable than the sequence that started with the protonation of the surface.

We highlight that the formed H_BO_B–V_B bond has a length of 1.79 Å and OP value of 0.534, similar to those of structural surface V–O bonds. The H–O bond formed by H chemisorption on the O_V—Sb_V site has a length of 0.97 Å and its OP value is 0.594. Meanwhile, the H–O bond formed by H interaction on the O_{Sb}—V_{Sb} also has a length of 0.98 Å. Note that in both cases the length of the OH bonds is similar to that in an isolated water molecule. The O_V and O_{Sb} atoms weakened about 20% its bonding interaction with the corresponding Sb_V or V_{Sb} cations due to the formation of the H–O bond. Therefore, this model will be useful for studying the interactions of different hydrocarbons and intermediate species on the V–Sb mixed oxide surface.

4. CONCLUSIONS

Density functional theory (DFT) calculations were performed in order to study the effect of V and Sb vacancies on vanadium

dx.doi.org/10.1021/jp4032805 | J. Phys. Chem. C 2013, 117, 20548–20556

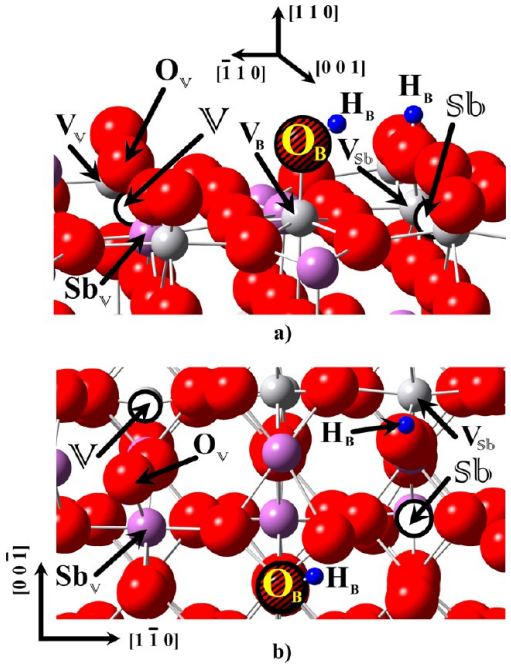

Figure 14. Brønsted acid site formation: (a) side view, (b) top view. Sequence OH (1st) then H.

antimonate surface properties. The nonstoichiometric $VSbO_4(110)$ surface, generated by cutting a 16.67% cation-deficient rutile-type bulk structure, exposed an extra oxygen layer and isolated V cations surrounded by Sb atoms. The introduction of V and Sb vacancies resulted in shortening of the nearest-neighbor cation metal-O bonds. The Bader charge results indicated that introduction of cation-defects is also reflected in the generation of oxidized V cations. The low-coordinated surface V^{4+} cations could act as Lewis acid sites. On the other hand, Brønsted acid sites were formed by the adsorption of the OH group on a V cation, while the H species preferentially interacted with an oxygen nearest-neighbor of an Sb vacancy. Density of states (DOS) plot of the non-stoichiometric $VSbO_4(110)$ surface showed O, V, and Sb bands located at different energy values. The DOS calculations did not reflect the characteristic band gap of TiO_2 (rutile) but the picture of vanadium dioxide (VO_2) with rutile-like structure. The top of the band between −8 eV and the Fermi level was mainly composed of V(3d) states and O(2p) orbitals coming from surface O atoms located close to a V vacancy. This fact suggested that surface oxygen atoms close to a V defect could be involved in hydrocarbons reactions.

AUTHOR INFORMATION

Corresponding Author

*E-mail: cajuan@criba.edu.ar.

Notes

The authors declare no competing financial interest.

ACKNOWLEDGMENTS

The authors gratefully acknowledge the financial support of Universidad de Buenos Aires (UBACYT-20020110200044), Universidad Nacional del Sur, CIC-BA, CONICET (PIP 11220090100785 and ANPCyT (PICT-2011-1312, 2010-1770 and 2186-2012). H.S. thanks CONICET for a doctoral fellowship.

REFERENCES

(1) Guerrero-Pérez, M. O.; Janas, J.; Machej, T.; Haber, A.; Lewandowska, A.; García-Fierro, J.; Bañares, M. A. Selective Destruction of Nitrogen-Containing Organic Volatile Compounds over Sb−V−O Catalysts. *Appl. Catal. B: Envirom.* **2007**, *71*, 85−93.

(2) Kim, B.; Park, D.; Kim, I.; Woo, H. Selective Oxidation of Hydrogen Sulfide over Mixture Catalysts of V−Sb−O and Bi_2O_3. *Catal. Today* **2003**, *87*, 11−17.

(3) Li, K.; Wu, K. Selective Oxidation of Hydrogen Sulfide to Sulfur on Vanadium-Based Catalysts Containing Tin and Antimony. *Ind. Eng. Chem. Res.* **2001**, *40*, 1052−1057.

(4) Zhang, H.; Zhang, J.; Sun, K.; Feng, Z.; Ying, P.; Li, C. Catalytic Performance of the Sb−V Mixed Oxide on Sb−V−O/SiO_2 Catalysts in Methane Selective Oxidation to Formaldehyde. *Catal. Lett.* **2006**, *106*, 89−93.

(5) Shishido, T.; Inoue, A.; Konishi, T.; Matsuura, I.; Takehira, K. Oxidation of Isobutane over Mo−V−Sb Mixed Oxide Catalyst. *Catal. Lett.* **2000**, *68*, 215−221.

(6) Guttmann, A.; Grasselli, R. K.; Brazdil, J. F. US Pat. 4, 746, 641, 4, 788, 317, 1988.

(7) Centi, G.; Marchi, F.; Perathoner, S. Effect of Ammonia Chemisorption on the Surface Reactivity of V−Sb-oxide Catalysts for Propane Ammoxidation. *Appl. Catal. A: General* **1997**, *149*, 225−244.

(8) Guerrero-Pérez, M. O.; Fierro, J. L. G.; Vicente, M. A.; Bañares, M. A. Effect of Sb/V Ratio and of Sb+V Coverage on the Molecular Structure and Activity of Alumina-Supported Sb−V−O Catalysts for the Ammoxidation of Propane to Acrylonitrile. *J. Catal.* **2002**, *206*, 339−348.

(9) Guerrero-Pérez, M. O.; Fierro, J. L. G.; Bañares, M. A. Effect of Synthesis Method on Stabilized Nano-Scaled Sb−V−O Catalysts for the Ammoxidation of Propane to Acrylonitrile. *Top. Catal.* **2006**, *41*, 43−53.

(10) Hamid, S.; Centi, G.; Pal, P.; Derouane, E. Site Isolation and Cooperation Effects in the Ammoxidation of Propane with VSbO and Ga/H-ZSM-5 Catalysts. *Top. Catal.* **2001**, *15*, 161−168.

(11) Grasselli, R. K.; Burrington, J. D.; Buttrey, D. J.; De Santo, P.; Langmuir, C. G. Multifunctionality of Active Centers in (Amm)-oxidation Catalysts: From Bi−Mo−Ox to Mo−V−Nb−(Te, Sb)−Ox. *Top. Catal.* **2003**, *23*, 5−22.

(12) Birchall, T.; Sleight, A. E. Oxidation States in Vanadium Antimonate ($VSbO_4$). *Inorg. Chem.* **1976**, *15*, 868−870.

(13) Hansen, S.; Stahl, K.; Nilsson, R.; Andersson, A. The Crystal Structure of $Sb_{0.92}V_{0.92}O_4$, Determined by Neutron and Dual Wavelength X-ray Powder Diffraction. *J. Solid State Chem.* **1993**, *102*, 340−348.

(14) Rojas, E.; Calatayud, M.; Bañares, M. A.; Guerrero-Pérez, M. O. Theoretical and Experimental Study of Light Hydrocarbon Ammoxidation and Oxidative Dehydrogenation on (110)-$VSbO_4$ Surfaces. *J. Phys. Chem. C* **2012**, *116*, 9132−9141.

(15) Larrondo, S.; Irigoyen, B.; Baronetti, G.; Amadeo, N. Vanadium Antimonate as a Partial Oxidation Catalyst. *Appl. Catal. A: General* **2003**, *250*, 279−285.

(16) Centi, G.; Mazzoli, P. Structure−Activity Relationship in Sb−V-Oxide Catalysts for the Direct Synthesis of Acrylonitrile from Propane. *Catal. Today* **1996**, *28*, 351−362.

(17) Andersson, A.; Andersson, S. L. T.; Centi, G.; Grasselli, R. K.; Sanati, M.; Trifiro, F. Surface Characterization and Reactivity in Ammoxidation Reactions of Vanadium Antimonate Catalysts. *Appl. Catal.* **1994**, *113*, 43−57.

(18) Roussel, H.; Mehlomakulu, B.; Belhadj, F.; van Steen, E.; Millet, J. M. M. Active Sites Characterization in Mixed Vanadium and Iron Antimonate Oxide Catalysts for Propane Ammoxidation. *J. Catal.* **2002**, *205*, 97−106.

(19) Irigoyen, B.; Juan, A.; Larrondo, S.; Amadeo, N. Adsorption Reactions of Toluene on the (110) Vanadium Antimonate Oxide Surface. *J. Catal.* **2001**, *201*, 169−182.

(20) Irigoyen, B.; Juan, A.; Larrondo, S.; Amadeo, N. The Adsorption of Toluene on V-Sb Oxides. Theoretical Aspects. *Surf. Sci.* **2003**, *523*, 252−266.

(21) Rojas, E.; Calatayud, M.; Guerrero-Pérez, M. O.; Bañares, M. A. Correlation between Theoretical and Experimental Investigations of the Ammonia Adsorption Process on the (110)-$VSbO_4$ Surface. *Catal. Today* **2010**, *158*, 178−185.
(22) Messina, S.; Juan, A.; Larrondo, S.; Irigoyen, B.; Amadeo, N. Theoretical Study of the Influence of Cation Vacancies on the Catalytic Properties of Vanadium Antimonate. *Appl. Surf. Sci.* **2008**, *254*, 5837−5843.
(23) Fujita, H.; Kanougi, T.; Atoguchi, T. Distribution of Brønsted Acid Sites on Beta Zeolite H-BEA: A Periodic Density Functional Theory Calculation. *Appl. Catal. A: General* **2006**, *313*, 160−166.
(24) Alberti, A. Location of Brønsted Sites in Mordenite. *Zeolites* **1997**, *19*, 411−415.
(25) Soyer, S.; Uzun, A.; Senkan, S.; Onal, I. A Quantum Chemical Study of Nitric Oxide Reduction by Ammonia (SCR Reaction) on V_2O_5 Catalyst Surface. *Catal. Today* **2006**, *118*, 268−278.
(26) Kresse, G.; Furthmüller, J. http://cms.mpi.univie.ac.at/vasp/vasp/vasp.html. (accessed Feb 2, 2013).
(27) Kresse, G.; Furthmuller, J. Efficiency of Ab-Initio Total Energy Calculations for Metals and Semiconductors Using a Plane-Wave Basis Set. *Comput. Mater. Sci.* **1996**, *6*, 15−50.
(28) Kresse, G.; Hafner, J. Ab Initio Molecular Dynamics for Liquid Metals. *Phys. Rev. B* **1993**, *47*, 558−561.
(29) Perdew, J. P.; Chevary, J. A.; Vosko, S. H.; Jackson, K. A.; Pederson, M. R.; Singh, D. J.; Fiolhais, C. Atoms, Molecules, Solids, and Surfaces: Applications of the Generalized Gradient Approximation for Exchange and Correlation. *Phys. Rev. B* **1992**, *46*, 6671−6687.
(30) Kresse, G.; Joubert, D. From Ultrasoft Pseudopotentials to the Projector Augmented-Wave Method. *Phys. Rev. B* **1999**, *59*, 1758−1775.
(31) Monkhorst, H. J.; Pack, J. Special Points for Brillouin-Zone Integrations. *Phys. Rev. B* **1976**, *13*, 5188−5192.
(32) Hoffmann, R., *Solids and Surfaces: A Chemist's View of Bonding in Extended Structures*; VCH: New York, 1988.
(33) Soler, J. M.; Artacho, E.; Gale, J. D.; García, A.; Junquera, J.; Ordejón, P.; Sánchez-Portal, D. The SIESTA Method for ab Initio Order-N Materials Simulation. *J. Phys.: Condens. Matter* **2002**, *14*, 2745.
(34) Berry, F. J.; Smart, L. E.; Duhalde, S. Titanium-Substituted Vanadium and Iron Antimonates. *Polyhedron* **1996**, *15*, 651−654.
(35) Centi, G.; Mazzoli, P.; Perathoner, S. Dependence of the Catalytic Behavior of V—Sb-Oxides in Propane Ammoxidation to Acrylonitrile from the Method of Preparation. *Appl. Catal., A* **1997**, *165*, 273−290.
(36) Callahan, J. L.; Grasselli, R. K. A Selectivity Factor in Vapor-Phase Hydrocarbon Oxidation Catalysis. *AIChE J.* **1963**, *9*, 755−760.
(37) Grasselli, R. K. In *Handbook of Heterogeneous Catalysis: Ammoxidation*; Ertl, G., Knoezinger, H., Weitkamp, J., Eds.; John Wiley and Sons: New York, 1997; Vol. *5*, p 2302.
(38) Haras, A.; Witko, M.; Salahub, D. R.; Hermann, K.; Tokarz, R. Electronic Properties of the VO_2 (011) Surface: Density Functional Cluster Calculations. *Surf. Sci.* **2001**, *491*, 77−87.
(39) Guelfucci, M. F. Electronic Calculations on Rutile VO_2 by the LMTO-ASA Method. *J. Phys. Chem. Solids* **2001**, *62*, 1961−1966.
(40) Wertheim, G. K.; Campagna, M.; Guggenheim, H. J.; Remeika, J. P.; Buchanan, D. N. E. X-ray Photoemission Study of Metal−Insulator Transitions in VO_2 V_2O_3 and NiS. *AIP Conf. Proc.* **1975**, *24*, 235−237.
(41) Mellan, T. A.; Grau-Crespo, R. Density Functional Theory Study of Rutile VO_2 Surfaces. *J. Chem. Phys.* **2012**, *137*, 154706 (1−8).
(42) Centi, G.; Marchi, F.; Perathoner, S. Surface Chemistry of V−Sb−Oxide in Relation to the Mechanism of AcrylonitrileS from Propane. Part 2. Reactivity towards Ammonia and Relationship with Catalytic Behavior. *J. Chem. Soc. Faraday Trans.* **1996**, *92*, 5151−5159.
(43) Henkelman, G.; Arnaldsson, A.; Jonsson, H. A Fast and Robust Algorithm for Bader Decomposition of Charge Density. *Comput. Mater. Sci.* **2006**, *36*, 354−360.
(44) Grasselli, R. K. Advances and Future Trends in Selective Oxidation and Ammoxidation Catalysis. *Catal. Today* **1999**, *49*, 141−153.
(45) Hammer, B.; Wendt, S.; Besenbacher, F. Water Adsorption on TiO_2. *Top. Catal.* **2010**, *53*, 423−430.
(46) Nisar, J.; Araujo, C. M.; Ahuja, R. Water Interaction with Native Defects on Rutile TiO_2 Nanowire: Ab Initio Calculations. *Appl. Phys. Lett.* **2011**, *98*, 083115 (1−3).
(47) Miao, M.; Liu, Y.; Wang, Q.; Wu, T.; Huang, L.; Gubbins, K. E.; Nardelli, M. B. Activation of Water on the TiO_2 (110) Surface: The case of Ti Adatoms. *J. Chem. Phys.* **2012**, *136*, 064703 (1−5).
(48) Lindan, P. J. D.; Harrison, N. M.; Gillan, M. J. Mixed Dissociative and Molecular Adsorption of Water on the Rutile (110) Surface. *Phys. Rev. Lett.* **1998**, *80*, 762−765.
(49) Lindan, P. J. D.; Zhang, C. Exothermic Water Dissociation on the Rutile TiO_2(110) Surface. *Phys. Rev. B* **2005**, *72*, 075439 (1−7).